Journal of Applied Polymer Science

Renewable thermoplastic multiphase systems from dimer fatty acids, with mineral microfillers

Marie Reulier,[1] Rodrigue Matadi Boumbimba,[2] Damien Rasselet,[1,3] Luc Avérous[1]

[1]BioTeam/ICPEES-ECPM, UMR CNRS 7515, Université De Strasbourg, 25 Rue Becquerel, Strasbourg Cedex 2, 67087, France

[2]Laboratory of Mechanics, Biomechanics, Polymers, and Structures, National Engineering School of Metz, 1 Route D'ars Laquenexy cs6582, Metz Cedex 3, 57078, France

[3]SOPREMA, 14 Rue De Saint Nazaire, CS 60121, Strasbourg Cedex, 67025, France

Correspondence to: L. Averous (E-mail: luc.averous@unistra.fr)

ABSTRACT: Renewable thermoplastic blends based on polyurethane (TPU) and polyamide (DAPA) obtained from dimers of fatty acids were reinforced with mineral microfillers, surface coated calcium carbonate ($CaCO_3$) or high aspect ratio talc (HAR), to prepare different micro-biocomposites systems. The influence of the nature of the filler, the aspect ratio and the filler content (5, 10, and 15 wt %), for different TPU/DAPA ratios (20/80, 50/50, and 80/20 wt %/wt %), were specifically investigated. Differential scanning calorimetry (DSC) and thermogravimetric analyses were conducted to investigate the thermal properties. DSC analyses showed that the addition of $CaCO_3$ had no influence on the glass transition and the melting temperature of the corresponding composites. Moreover, the morphology and the mechanical properties in the solid state of the different multiphase systems were investigated. SEM observations after tensile tests showed that the best matrix/filler interactions were obtained in the case of the 20/80-based systems. Uniaxial tensile tests have shown that the addition of HAR or $CaCO_3$ fillers led to a clear increase of the Young modulus. Micromechanical models based on a two-phase composite approach, including Mori–Tanaka and Davies models were used to describe the dependence of the elastic modulus on the volume fraction of HAR or $CaCO_3$ fillers. © 2015 Wiley Periodicals, Inc. J. Appl. Polym. Sci. **2016**, *133*, 43055.

KEYWORDS: biopolymers and renewable polymers; composites; mechanical properties; thermal properties; thermoplastics

Received 2 September 2015; accepted 16 October 2015

DOI: 10.1002/app.43055

INTRODUCTION

Nowadays, the use of renewable bio-based carbon feedstock is of considerable interest because it offers the intrinsic value of a reduced carbon footprint and an improved life cycle analysis, in agreement with a sustainable development. In this way, polymers with new macromolecular architectures are more and more often obtained from biomass through different chemical and/or biochemical processes.[1] These bio-based materials with controlled chemical architectures represent a good alternative to conventional and fossil based chemical feedstock. Thermoplastic polyurethane (TPU) and polyamide (DAPA) obtained from fatty acid stand as good candidates. Recently, our group has demonstrated that TPU and DAPA could be prepared from dimers of fatty acids.[2–5] TPUs are thermoplastic elastomers formed of hard segments (HS) linked together by intermolecular hydrogen bonds, which act as physical crosslinkers, associated to soft segments (SS) contributing to the elastomeric behavior. HS and SS are organized into segregated domains or microphases with the specific behavior of a thermoplastic elastomer i.e., high and reversible elongations.[5] Compared to TPU, DAPA shows the conventional behavior of a classic semi-crystalline thermoplastic, however DAPA is more flexible than most of the conventional polyamides.[6]

While there is a growing interest in using TPU or DAPA alone, their corresponding applications are still limited due to their reduced thermal and mechanical properties. A very recent study on TPU/DAPA blends has shown the promise interest of this association.[7] At the processing shear rate, the apparent viscosities of each polymer have similar values allowing a good dispersion of each phase, leading to rather isotropic materials. Different morphologies can be obtained according to the TPU/DAPA ratio. For instance, for a ratio close to one a co-continuous structure was observed. However, the final mechanical properties of those blends still need to be improved e.g., by addition of fillers.

Addition of fillers such as calcium carbonate ($CaCO_3$) is commonly used to tailor mechanical properties such as strength and

Additional Supporting Information may be found in the online version of this article.

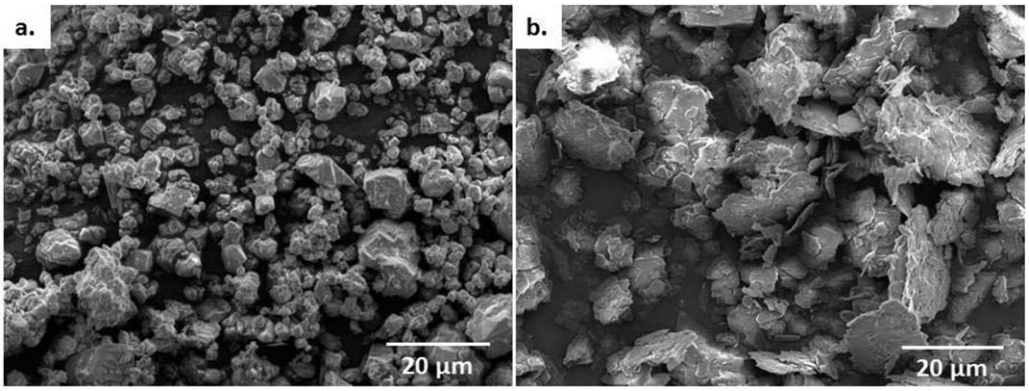

Figure 1. SEM observations of neat (a) $CaCO_3$ and (b) HAR at the same scale (bar = 20 µm).

modulus with a reduction of the material cost. Because of low filler–matrix interactions,[8] many attempts were carried out to improve the compatibility at the interface using, for instance, silane grafted onto the filler or fatty acid treatment.[9,10]

Studies on talc-filled polymers have also been widely investigated.[11–13] Because of its lamellar shape, talc can bring specific mechanical properties. To increase the surface and the aspect ratio of the particles and to obtain microfillers (micron-sized), a delamination process is now commonly used. The corresponding natural talc-based microparticles present a high aspect ratio with an average thickness of some hundreds of nanometers, based on stacked platelets.[14]

The aim of this study was to prepare new bio-based microcomposites with different TPU/DAPA ratios and, talc or $CaCO_3$ as fillers. Composites with different filler contents were prepared. The effects of the shape, aspect ratio, and filler content on the morphology and the thermal and mechanical properties of the final composites were investigated. Micromechanical models based on a two-phase composite, including Mori–Tanaka[15] and Davies[16] models were used to predict the elastic properties of these composites, and then compared with the experimental data.

EXPERIMENTAL

Materials

Chemicals and Compounds. The bio-based polyester polyol used in this study was kindly supplied by Oleon (France). The polyol is based on dimeric fatty acids from rapeseed oil, with a purity higher than 98%, a hydroxyl value of 33 mg.(g KOH)$^{-1}$ and a weight average molar mass of around 3300 g mol^{-1}. The 4,4′-diphenylmethane diisocyanate (MDI) was supplied by Brenntag (France) and 1,4-butanediol (BDO) was purchased from Sigma–Aldrich (France). DAPA has been provided by Arkema (France), under the trade name of Platamid HX. DAPA is a semi-crystalline polymer, with a glass transition (T_g) at 6°C and a melting temperature (T_m) of 120°C. The high aspect ratio natural talc used in this study (HAR), was supplied by Imerys Talc (France). HAR particles have been obtained by delamination of coarse natural talc leading to micron-sized particles [Figure 1(b)]. The HAR medium particle size d50 determined by laser diffraction is about 10 µm with a specific surface area of 19.5 m^2 g^{-1}. A fatty-acid-coated calcium carbonate, designated here as $CaCO_3$, with a medium particle size d50 of 6.5 µm and a specific surface area of 1.3 m^2 g^{-1} was provided by Omya (France) [Figure 1(a)]. Phenol, 1,2-dichlorobenzene and dimethylformamide were used without any further purification.

TPU synthesis. TPU was prepared with an isocyanate/hydroxyl (NCO/OH) ratio equal to 1 and HS content of 17 wt %, by a two-step process. During the first step, a prepolymer with NCO ending groups is obtained. In a second step, the high molar mass TPU is prepared with BDO, as a chain extender. After polymerization, the system was cured overnight in an oven at 70°C to ensure the complete reaction of NCO groups. NCO content was evaluated in order to follow the reaction kinetics during the different steps. The detailed synthesis has been fully described in a previous publication.[5] The corresponding TPU showed a glass transition of −48°C, which is related to the SS.

Preparation of the Blends and Composites. Prior to melt mixing, the TPU and DAPA pellets as well as the microfillers were dried overnight at 70°C, under vacuum. The composites were prepared using an internal mixer (Counter-rotating mixer Rheomix 600p, Haake, USA) equipped with a pair of high-shear roller-type rotors at 150°C with a speed of 80 rpm for 8 min. After melt processing, the composites were compression-molded, to obtain films or sheets, with a hot press at 160°C applying 160 MPa pressure for 5 min and further squeezed between two steel plates for 5 min.

The weight ratios (wt %/wt %) of the TPU/DAPA systems were 80/20, 50/50 and 20/80, respectively. All the composites present the corresponding designations: TPU/DAPA (X/Y)_Filler Z, where X/Y is equal to the TPU/DAPA weight ratio, with $X + Y = 100$. Filler can be HAR or $CaCO_3$, respectively, and Z can be 5, 10, or 15, corresponding to the filler weight ratio. An example is "TPU/DAPA (80/20)_HAR 10" or "(80/20)_HAR 10", corresponding to a composite where the weight ratio of the TPU/DAPA system is 80/20 (wt %/wt %) and the HAR content is 10 wt %.

General Methods

Thermogravimetric analyses (TGA) of the polymer blends i.e., the systems without fillers, and the composites were performed on a Hi-Res TGA 2950 apparatus from TA Instruments. Samples were heated from room temperature up to 700°C at a rate of 20°C min^{-1}, under air flow.

Table I. Surface Tension, Polar, and Dispersive Components of Test Liquids

	Surface tension energy (mJ m^{-2})	γ polar (mJ m^{-2})	γ dispersive (mJ m^{-2})
Diiodomethane	50.8	2.3	48.5
Water	72.8	51.0	21.8

Differential scanning calorimetry (DSC) was performed using a TA Instruments Q 200 under nitrogen (flow rate 50 mL min^{-1}). All samples were weighed between 2 and 5 mg. The samples were heated up to 160°C with a heating rate of 10°C min^{-1} (first heating scan), then cooled down to −80°C at 10°C min^{-1} and finally reheated to 160°C at a heating rate of 10°C min^{-1} (second heating scan). Previously and by TGA, the control that no major degradation could take place in this explored temperature range has been performed. The glass transition (T_g) and the melting (T_m) temperatures were determined at the midpoint of the change in the slope of the baseline and the maximum of the melting point, respectively. These values were determined on the second heating scan since the first scan serves only to erase any previous thermal history. The phase crystallinity is determined by eq. (2), where $\Delta H_{m0} = 190$ J g^{-1} for 100% crystalline DAPA,[17] w is the DAPA weight percentage in the blend, ΔH_m corresponds to the melting enthalpy and ΔH_{cc} is the enthalpy of crystallization preceding melting.

$$X_{DAPA}(\%) = \frac{\Delta H_m - \Delta H_{cc}}{\Delta H_{m0} \times w} \times 100 \quad (1)$$

The surface tension (Gibbs free energy per surface area) gives an indication of the intermolecular forces at the interface. It was obtained by contact angle measurements. Wu's method,[18,19] particularly adapted to low energy systems, allowed the calculation of the polar (γ^p) and dispersive (γ^d) components of the surface energy (γ). Then, the interfacial tension γ_{12} and thermodynamic work of adhesion W_{12} between each component were calculated according to the harmonic mean eqs. (2) and (3)[20]:

$$\gamma_{12} = \gamma_1 + \gamma_2 - 4\left(\frac{\gamma_1^d \gamma_2^d}{\gamma_1^d \times \gamma_2^d} + \frac{\gamma_1^p \gamma_2^p}{\gamma_1^p \times \gamma_2^p}\right) \quad (2)$$

$$W_{12} = 4\left(\frac{\gamma_1^d \gamma_2^d}{\gamma_1^d \times \gamma_2^d} + \frac{\gamma_1^p \gamma_2^p}{\gamma_1^p \times \gamma_2^p}\right) \quad (3)$$

Surface tension of HAR, DAPA, and TPU was determined with the sessile drop method on a GBX Digidrop R&D LC goniometer (France). A droplet was deposited onto the surface of a plate sample. Water and diiodomethane were used as test-liquids because of their different polarities (Table I).

Scanning electron microscopy (SEM), on a TESCAN Vegan 3 (Czech Republic) with a 10 kV accelerating voltage was used to examine the dispersed phase distribution, and to localize both talc and calcium carbonate microparticles. Samples were obtained after cryogenic fracture in liquid nitrogen. To specifically observe the phase distributions of the polymers, selective extractions were performed using formic acid 95%, when DAPA was the dispersed phase, or a dimethylformamide//phenol/1,2-dichlorobenzene solution 1.0/0.1/0.9 in volume when TPU was the minor phase. The extractions were carried out at room temperature for 48 h. All surfaces were gold-coated on a Quorum Technology Gold Coater Sputter.

Uniaxial tensile tests were carried out with an Instron 5585H (USA) equipped with a load cell of 5 kN. The experiments were performed at room temperature at a constant strain rate of 10^{-2} s^{-1} on samples with dimensions of 20 mm × 4 mm × 1 mm. Young's modulus (E), tensile strength at break (σ_{max}) and elongation at break (ε_{max}) were determined. The yield point is defined as the maximum of the stress–strain curve before softening.

RESULTS AND DISCUSSION

Morphology of TPU/DAPA Composites

SEM images of the cryogenically fractured surface of the (80/20) blend and the composites are shown in Figures 2–4. In agreement with previous publications on TPU/DAPA blends from fatty acid dimers,[7] in the case of 80/20 blends, DAPA phases are well dispersed into the TPU matrix as observed in Figure 2. The average size of the dispersed DAPA phase is 0.9 ± 0.2 µm.

In Figure 3, the dispersion of $CaCO_3$ at a concentration of 15 wt % is observed for the different TPU/DAPA ratios. $CaCO_3$ is well dispersed in each case. Figure 3(a) shows that due to its size, $CaCO_3$ is mainly localized in the major phase for the lowest and highest TPU/DAPA ratios, 80/20 and 20/80, respectively. For the 80/20 composite it is also possible to measure the size of the DAPA particles. We observed that the addition of $CaCO_3$ does not modify the initial morphology of the blend as observed in Figure 2. The corresponding dispersed DAPA phase exhibits an average size of 0.8 ± 0.2 µm, i.e. similar to the initial value.

Figure 4 shows the dispersion of the HAR for the different TPU/DAPA ratios. HAR particles are well dispersed and, as expected for $CaCO_3$, these particles are also well distributed into the major phase for 80/20 and 20/80 systems (Figure 4). Partial voids can be noticed between the HAR platelets and the matrix for 80/20-based composites [Figure 4(b)], demonstrating

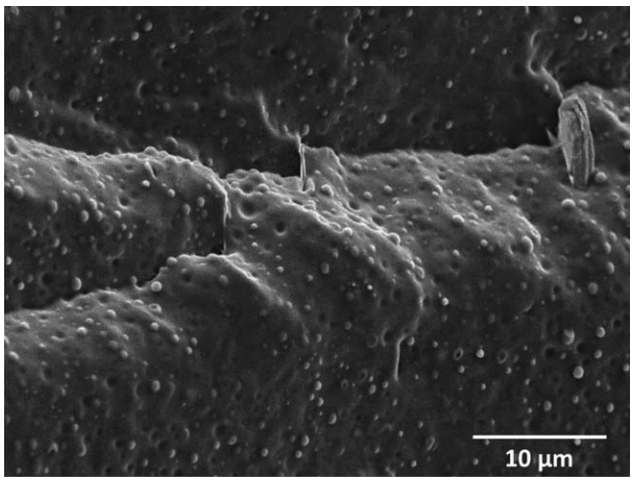

Figure 2. SEM image of TPU/DAPA blend at a weight ratio of 80/20 after a cryogenic fracture.

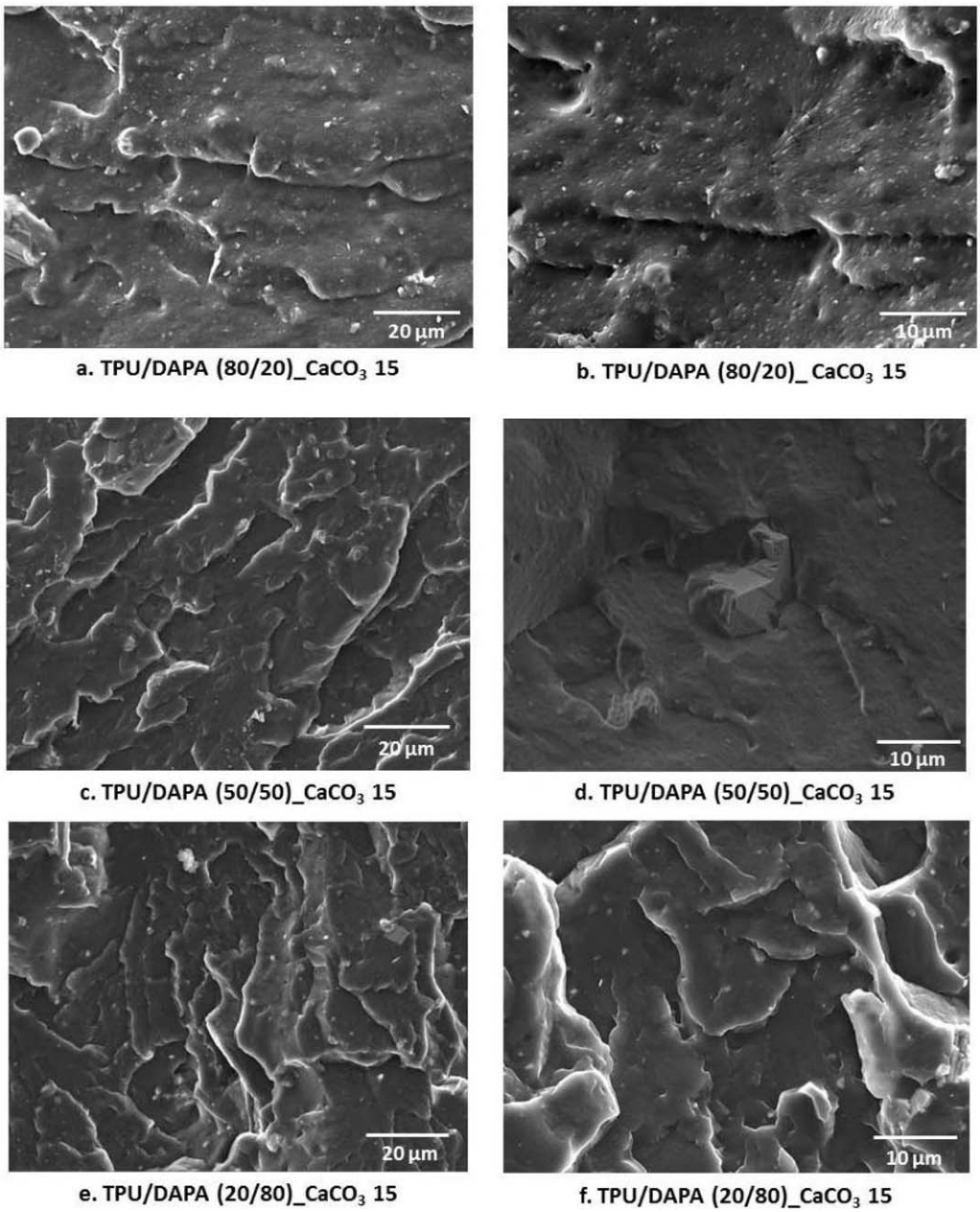

Figure 3. SEM images after a cryogenic fracture of TPU/DAPA composites based on 15 wt % of $CaCO_3$.

a poor TPU-HAR affinity. For this specific TPU/DAPA ratio, the DAPA phase displays an average size of 0.8 ± 0.2 µm, i.e. similar to the initial size.

No clear conclusions can be drawn regarding the separation of $CaCO_3$ or HAR micro-particles into one of the phases (DAPA vs. TPU) from the SEM images for the TPU/DAPA (50/50) systems. However, it is possible to theoretically predict the location of solid fillers in immiscible polymer blends[21] (Supporting Information).

Mixing procedures have a direct impact on the filler location.[22] In our case $CaCO_3$ or HAR are introduced into the blends, one of the key parameters to take into account is then the viscosity of the different polymer phases in the melted blend. It has however been previously reported[7] that TPU and DAPA display similar viscosities under the conditions of the mixing process. With this in mind, the location of the fillers will be, therefore, mostly dependent on the interfacial tension values. The calculated wetting coefficient values of $CaCO_3$ and HAR, at room temperature, are 3.4 and −0.4, respectively, which would suggest that $CaCO_3$ is mainly located in the DAPA phase and HAR at the DAPA/TPU interface. After cryogenic fracture, selective extractions and TGA analyses, it appears that HAR particles are preferentially located at the interface, as predicted. In addition, we can show that $CaCO_3$ microparticles are mainly dispersed into the DAPA phase. All the theoretical values obtained from the wetting coefficients calculated from surface tensions values (Supporting Information) are in good agreement with the experimental observations.

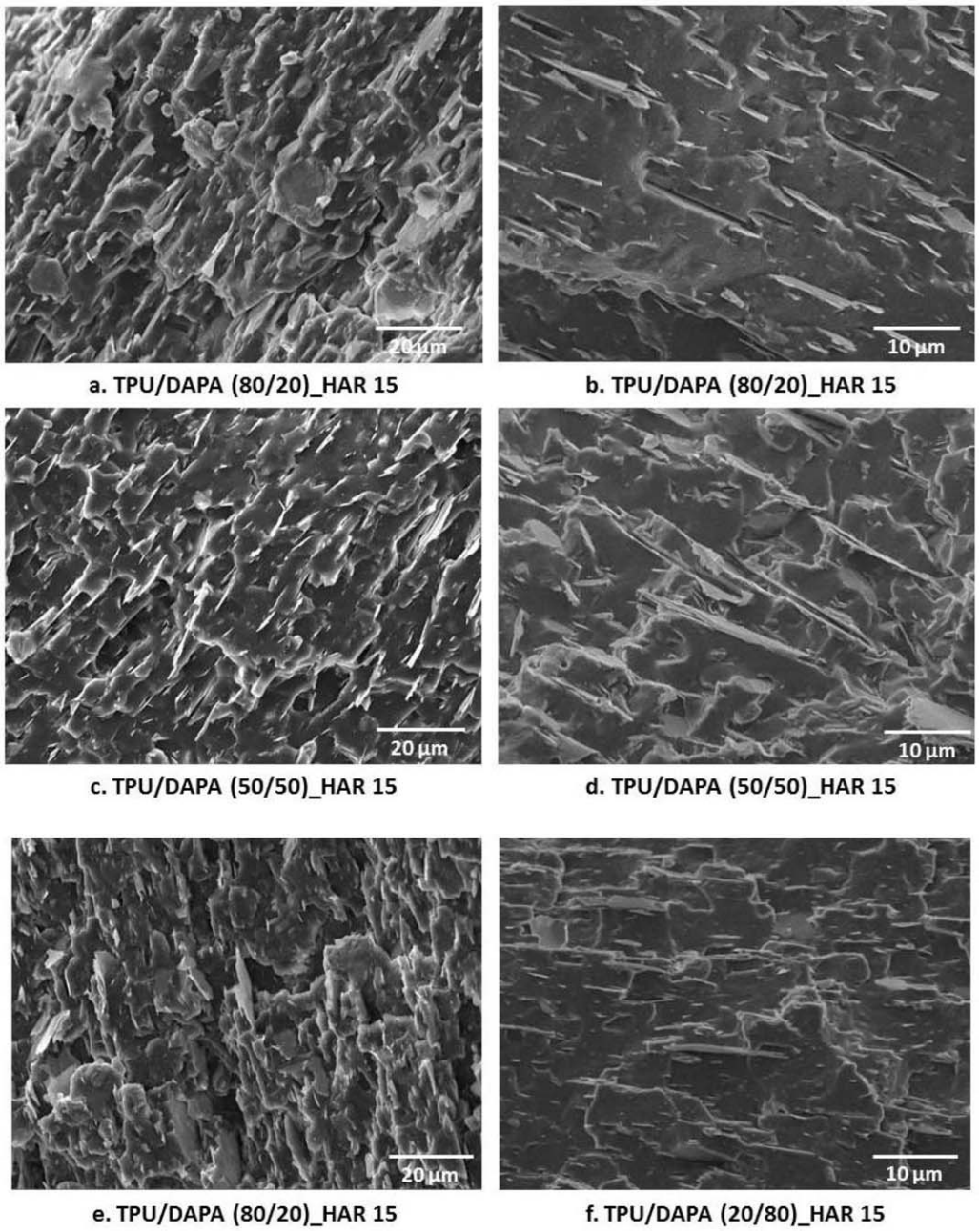

Figure 4. SEM images after a cryogenic fracture of TPU/DAPA composites based on 15 wt % of HAR.

Thermal Properties

Thermal degradation temperatures of the neat polymers and the (50/50) blend were determined by TGA. The corresponding thermograms under air are depicted in Figure 5. $T_{98\%}$, $T_{2\%}$, T_{DTGmax} as well as the mass losses are summarized in Table II. The TGA thermogram of TPU reveals three main degradation steps as described in the literature. Urethane groups are relatively thermally unstable[23,24] beginning to degrade around 150°C. This degradation then becomes irreversible at around 200°C (Supporting Information Figure 3). It has been reported[23,25] that the first degradation step is related to the urethane bond decomposition into isocyanate and alcohol with a possible formation of primary and secondary amines. It should be also specified that the mass loss associated with this first degradation step may also be correlated with the HS content. The second observed degradation step is related to the break of the ester bonds within the polyol soft phase of the TPU.[26] Finally, the third degradation step is related to the degradation of the residues produced during the second degradation and other fragments from the remaining structure.[2,4] DAPA mainly exhibits a unique degradation step starting at 377°C, as shown in Figure 5(a). According to the TGA thermogram, the maximum degradation temperature occurs at 448°C. Previous work[3] with similar DAPAs suggests that equivalent mechanisms occurring in PA 6 or 6-6 could be expected. Thus, the DAPA decomposition could start with the degradation of the alkylamide bond followed by the degradation of the major

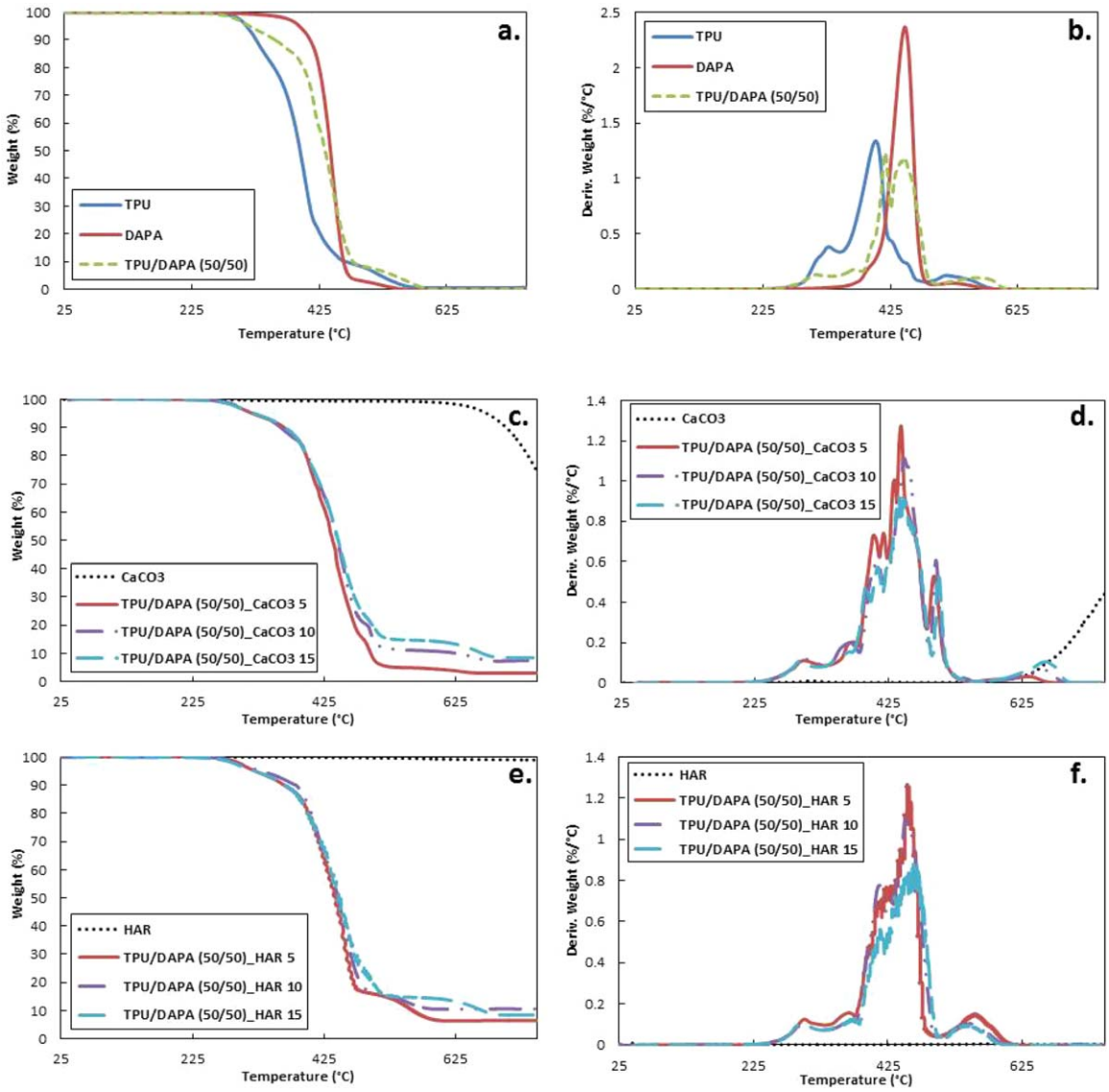

Figure 5. TGA and DTG curves for the neat fillers and the different composites. [Color figure can be viewed in the online issue, which is available at wileyonlinelibrary.com.]

components of the chains, the alkyl units. At the end of the TGA analyses, the thermal stability of DAPA is higher than TPU.

The thermal degradation of the (50/50) blend starts approximately at the same temperature as neat TPU (Table II). The global TGA curve of the blend shows the combination of the degradation steps of both main components [Figure 5(a)].

The thermal stability of HAR and $CaCO_3$ is reported in [Figure 5(c,e)]. The HAR shows a high thermal stability within the studied temperature range. Only a small mass loss (around 1 wt %) can be seen before 600°C that corresponds to the decomposition of chlorite and calcite impurities contained in the talc.[27] $CaCO_3$ exhibits a small weight loss of about 0.5%, starting at 274°C [Figure 5(c)]. This small degradation corresponds to the decomposition of the fatty acid used for the surface treatment. This value is in good agreement with the one given by Omya. The second degradation step is related to the decarbonation of the $CaCO_3$.[28]

Table II. Main Degradation Temperatures of the Neat Polymers and TPU/DAPA (50/50) Blend

	$T_{98\%}$ (°C)	$T_{2\%}$ (°C)	T_{DTGmax} (°C)/% of weight loss during the corresponding degradation step			
DAPA	377	526	448/96			
TPU	298	540	330/18	400/73	521/9	
(50/50) Blend	294	571	332/14	417/27	444/50	564/9

Table III. Filler Content (in wt %) Determined by TGA, for the TPU/DAPA (50/50)-based Composites

	$CaCO_3$ content	HAR content
(50/50)_filler 5	5	6
(50/50)_filler 10	11	11
(50/50)_filler 15	15	15

TGA analyses are also used to determine the final filler content. All the values obtained for the (50/50) composites are listed in Table III.

T_g, crystallization temperature (T_c), cold crystallization temperature (T_{cc}) which corresponds to the crystallization preceding melting, T_m of the TPU, DAPA, and the TPU/DAPA-based blends or composites, and the associated enthalpies (ΔH_c, ΔH_{cc}, and ΔH_m) obtained by DSC are presented in Table IV. DAPA is a semicrystalline polymer with a T_c at 39°C and a crystallinity content of about 4.1%. This crystallinity changes by blending with an increasing amount of TPU. Different possible explanations can be provided. It may be due to an overlapping of the DAPA cold crystallization and melting (Supporting Information Figure 2). Similar observations were reported e.g., for TPU/PLA blends.[29] An assumption, which needs to be verified with additional tests, could be that the HS of TPU interacts with the DAPA leading to an increase in T_c. Thus, TPU could act as a nucleating agent through its HS parts. When TPU was blended with DAPA it was observed that the crystallization takes place at a higher temperature as reported in the literature for different blends, such as TPU/PA1010 or TPU/aliphatic polyester.[30,31]

In the case of $CaCO_3$-based composites (Table IV), the T_g from TPU (SS), the T_g and T_m from DAPA stay constant when the microfiller is added. This is in agreement with previous observations on micro-calcium carbonate-based systems.[12] However, when $CaCO_3$ is added into the (80/20) systems, the crystallization temperature increases by 10 and 11°C for the composites with 5 and 15 wt % of microfiller, respectively, compared to the corresponding blend. No significant variations are noticed for the others TPU/DAPA ratios. Moreover, the crystallinity contents of the $CaCO_3$-based composites appear to be lower than the associated neat blends (Table IV). As a result, $CaCO_3$, which was assumed to be principally located in the DAPA phase for the (50/50)_$CaCO_3$ and the (20/80)_$CaCO_3$ systems, may restrict and prevent the crystal growth of the DAPA phase.

In the case of HAR-based composites, Table IV shows no impact on the T_g of TPU (SS), and T_g and T_m of the DAPA phase. For each composite, T_c occurs at a higher temperature than the corresponding neat blend. Similar trends were previously reported with natural talc added into PP/PA6 blend.[32] The addition of HAR microparticles also led to the

Table IV. Thermal Properties of the Neat Polymers, Blends, and the Different Composites

	$T_{g\ TPU}$ (°C)	$T_{g\ DAPA}$ (°C)	$T_{c\ DAPA}$ (°C)	$\Delta H_{c\ DAPA}$ (J g^{-1})	$T_{m\ DAPA}$ (°C)	$\Delta H_{m\ DAPA}$ (J g^{-1})	$T_{cc\ DAPA}$ (°C)	$\Delta H_{cc\ DAPA}$ (J g^{-1})	$X_{c\ DAPA}$ (%)
TPU	−48	-	-	-	-	-	-	-	-
DAPA	-	6	39	3.9	122	20.4	40	12.7	4.1
(80/20) Blend	−47	4	44	5.8	121	7.9	42	1.0	18.2
(80/20)_$CaCO_3$ 5	−48	4	54	0.8	120	4.3	46	2.7	4.3
(80/20)_$CaCO_3$ 10	−48	7	n.a.	n.a.	120	3.4	45	2.5	2.8
(80/20)_$CaCO_3$ 15	−48	5	55	0.9	119	3.7	47	2.0	5.1
(80/20)_HAR 5	−47	5	52	2.6	120	4.5	47	0.8	10.2
(80/20)_HAR 10	−49	7	59	2.7	121	3.8	n.a.	n.a.	11.1
(80/20)_HAR 15	−49	4	58	1.8	121	3.4	n.a.	n.a.	10.5
(50/50) Blend	−46	5	44	5.8	122	13.2	43	1.3	12.5
(50/50)_$CaCO_3$ 5	−47	6	41	1.2	120	9.7	45	6.9	3.2
(50/50)_$CaCO_3$ 10	−48	5	43	4.0	120	8.7	43	4.8	4.7
(50/50)_$CaCO_3$ 15	−47	5	40	1.3	119	9.2	44	6.6	3.2
(50/50)_HAR 5	−49	5	55	7.9	120	11.5	n.a.	n.a.	12.7
(50/50)_HAR 10	−48	5	63	10.3	122	10.3	n.a.	n.a.	12.0
(50/50)_HAR 15	−48	6	60	6.7	120	10.0	n.a.	n.a.	12.4
(20/80) Blend	−48	6	46	10.2	120	18.1	39	4.3	9.1
(20/80)_$CaCO_3$ 5	n.a.	4	40	2.0	119	15.1	43	11.7	2.4
(20/80)_$CaCO_3$ 10	n.a.	5	43	6.3	120	16	42	7.7	6.1
(20/80)_$CaCO_3$ 15	n.a.	4	40	2.3	119	14.5	44	9.4	4.0
(20/80)_HAR 5	−49	6	54	12.6	121	18.3	n.a.	n.a.	12.7
(20/80)_HAR 10	−49	3	56	12.1	118	17.4	n.a.	n.a.	12.7
(20/80)_HAR 15	−49	4	60	11.2	120	15.4	n.a.	n.a.	11.9

disappearance of the cold crystallization. This may be related to the rate of crystallization of the DAPA phase.[32] Crystallinity content of the (80/20) composites was reduced compared to the corresponding blend (Table IV). The reduction of the crystallinity content in PA6/talc composites was also reported.[33] They supposed that the mobility of the PA6 chains might be restricted during cooling. This phenomenon is also likely occurring in the case of our HAR and $CaCO_3$ composites. For (50/50)-based systems, crystallinity degrees are equivalent with or without HAR, and still above the values determined for equivalent $CaCO_3$-based composites. Increases in T_c combined with the rise of the phase crystallinity is only observed for the TPU/DAPA (20/80)_HAR systems. The crystallinity is around 3% higher than the corresponding blends for the different composites. This slight evolution could be due to a better distribution of the DAPA crystals and the presence of DAPA crystals with better degrees of perfection as explained by Bajsić *et al.*[34] for TPU/PP composites filled with talc. Furthermore, it has been assumed before that HAR particles may be located mainly in the DAPA phase for (20/80)_HAR systems. Thus, for this TPU/DAPA ratio in particular, HAR particles could be considered as nucleating agents.

Mechanical Properties

The main results from uniaxial tensile tests are present in Table V. The different corresponding stress–strain curves are presented in the Supporting Information (Supporting Information Figures 3 and 4). At high TPU content, two stages can be observed with an initial linear elasticity followed by a nonlinear transition to global yield stress (typical of elastomeric polymer materials). At high DAPA content, four stages can be distinguished, an initial linear elasticity, a non-linear transition to yield stress, the strain softening and the strain hardening (typical of many conventional thermoplastics).

The stress–strain curves of TPU/DAPA_HAR composites are presented in Supporting Information Figure 3. As described for the blends, the stress–strain curves of TPU/DAPA_HAR composites can be divided in different stages, depending on the TPU/DAPA ratio. The Young's modulus, the yield stress and the elongation at break of HAR-based composites systems are listed in Table V. It has been observed that for all the different neat blends, the Young's modulus value increases with the DAPA content due to the higher modulus of DAPA, compared to TPU. Moreover, the Young's modulus increases when the HAR concentration increases. The largest improvement is observed for the (20/80)_HAR systems. For these composites, the SEM images have shown that the HAR particles were mostly located in the DAPA phase, which increases the reinforcing effect introduced by the HAR. Moreover, this increase is also related to the highest crystallinity content of the DAPA.[32] In the same way, the yield stress also increases with the addition of HAR, especially at high DAPA content.

As for TPU/DAPA_HAR, the stress-strain curves of TPU/DAPA_$CaCO_3$ composites (Supporting Information Figure 4) reveal two stages for low DAPA concentration in TPU/DAPA matrix and four stages when the DAPA concentration increases. Young's modulus and yield stress increase with the $CaCO_3$ content. The largest increase appears when the DAPA content is the highest (Table V). Compared to HAR-based composites however, this improvement is lower. This is mainly due to the shape and higher aspect ratio of HAR, with an interfacial surface around 15 times greater than $CaCO_3$. Moreover, for the (20/80)_$CaCO_3$ systems, the crystallinity of the DAPA phase is lower than in the associated HAR-based systems, thus, the stiffness is less impacted.

Table V. Young Modulus, Yield Stress, and Elongation at Break of TPU/DAPA_HAR Systems

Multiphase systems	Young modulus (MPa)	Yield stress (MPa)	Elongation at break (%)
(80/20) Blend	4.4 ± 0.1	2.3 ± 0.2	389 ± 95
(80/20)_$CaCO_3$ 5	4.8 ± 0.3	2.4 ± 0.1	442 ± 16
(80/20)_$CaCO_3$ 10	4.6 ± 0.1	2.5 ± 0.2	412 ± 44
(80/20)_$CaCO_3$ 15	5.4 ± 0.1	2.5 ± 0.1	375 ± 28
(80/20)_HAR 5	5.2 ± 0.3	2.5 ± 0.1	351 ± 19
(80/20)_HAR 10	6.9 ± 0.2	2.6 ± 0.2	279 ± 16
(80/20)_HAR 15	10.2 ± 1.2	3.2 ± 0.1	237 ± 13
(50/50) Blend	45.6 ± 2.6	4.0 ± 0.1	460 ± 29
(50/50)_$CaCO_3$ 5	51.7 ± 3.3	5.3 ± 0.3	575 ± 43
(50/50)_$CaCO_3$ 10	56.0 ± 2.2	4.8 ± 0.1	400 ± 44
(50/50)_$CaCO_3$ 15	54.9 ± 1.9	5.7 ± 0.3	373 ± 22
(50/50)_HAR 5	53.2 ± 4.0	4.7 ± 0.1	300 ± 51
(50/50)_HAR 10	74.9 ± 8.4	6.2 ± 0.1	342 ± 24
(50/50)_HAR 15	107.1 ± 7.6	7.2 ± 0.1	209 ± 63
(20/80) Blend	70.0 ± 3.6	8.7 ± 0.2	845 ± 93
(20/80)_$CaCO_3$ 5	102.9 ± 5.3	9.4 ± 0.5	811 ± 110
(20/80)_$CaCO_3$ 10	120 ± 6.2	9.8 ± 0.7	795 ± 60
(20/80)_$CaCO_3$ 15	119.8 ± 2.8	10.2 ± 0.5	707 ± 49
(20/80)_HAR 5	135.4 ± 5.7	10.1 ± 0.3	718 ± 120
(20/80)_HAR 10	153.3 ± 12.3	11.2 ± 0.4	607 ± 87
(20/80)_HAR 15	183.2 ± 8.7	12.2 ± 0.1	464 ± 20

Analysis of Mechanism of Deformation. SEM observations performed on samples, which were ruptured during the tensile tests, provide some details on the mechanism of deformation of these composites. According to the corresponding SEM images, (80/20)_HAR systems [Figure 6(c) and Supporting Information Figure 6(c)] present a specific surface, which can be associated to a ductile break. The TPU/DAPA (80/20) matrix deforms as if it were subjected to shear yielding. As shown by SEM, the deformation process seems to be dominated by a succession of microvoid nucleation, growing and coalescence. Some microvoids are associated with completely dewetted HAR particles. The presence of micro-fibrils, related to the stretching of the predominant TPU phase, also appears on the SEM image. The interfacial debonding between HAR particle and TPU/DAPA (80/20) matrix is strongly supported, as previously mentioned, by the limited microfiller-TPU affinity. When DAPA content increases, the fracture surface stays representative of a ductile material, for instance for the (20/80) systems, however the SEM

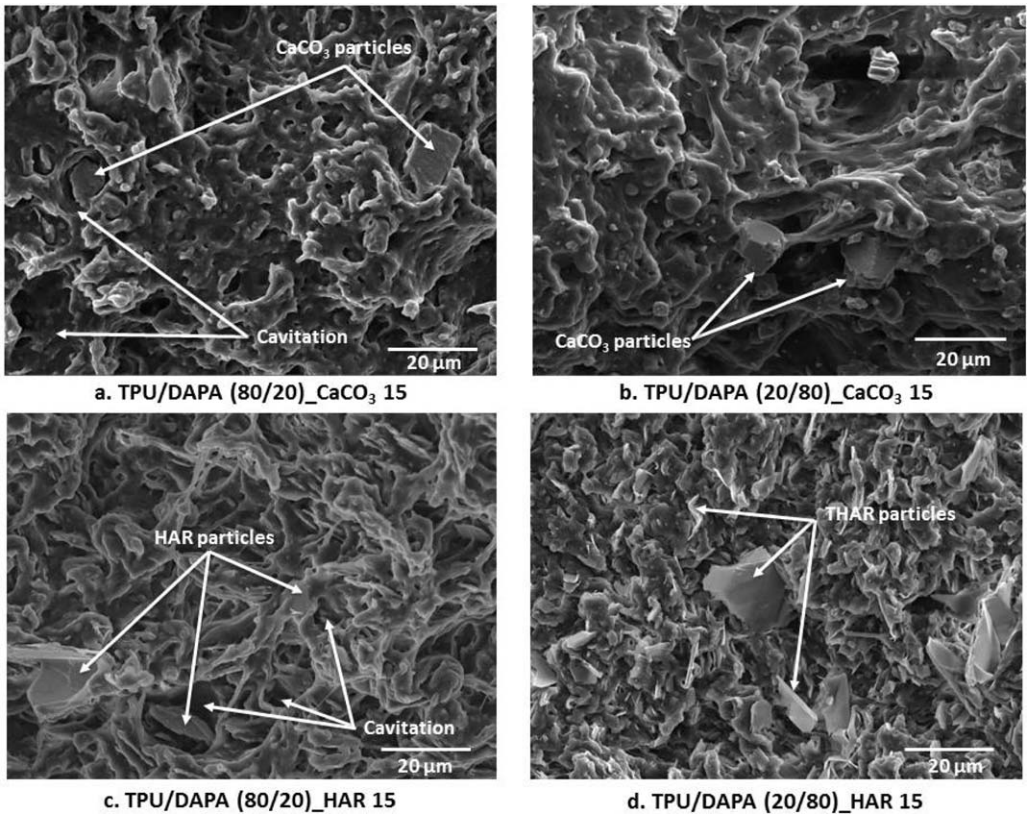

Figure 6. SEM images of TPU/DAPA systems filled with 15 wt % of $CaCO_3$ or HAR after a tensile fracture.

image [Figure 6(d) and Supporting Information Figure 6(d)] shows few microvoids in this case. The HAR–matrix interface shows good adhesion, in this case, the main deformation process is the shear yielding of the matrix.

The SEM images from (80/20)_$CaCO_3$ and (20/80)_$CaCO_3$ composites are shown in Figure 6 and Supporting Information Figure 6. The SEM picture of (80/20)_$CaCO_3$ [Figure 6(a)] reveals a rough surface, and it can be clearly seen that the $CaCO_3$ microparticles are completely dissociated from the (80/20) matrix. The SEM image also reveals some large voids specific to TPU cavitation. For this composite, the first mechanism of deformation seems to be based on the decohesion between the microfiller and the (80/20) matrix. When the strain increases, the rubbery TPU phase mainly deforms by cavitation, however, the DAPA phase deforms by matrix yielding (visible on the SEM picture as elongated fibrils). For the (20/80) system [Figure 6(b)], the SEM surface is smooth and presents many ductile fibrils. No dissociated particles are observed.

Modeling of the Elastic Properties. The modeling of the effect of the microfiller content on the elastic properties is performed by different micromechanical approaches. The effective properties of the composites could be predicted using a homogenization technique. The composite material is assumed to be a biphasic material composed of an homogeneous isotropic matrix (denoted *M*) with an elastic tensor $\boldsymbol{C}^{M}$ filled with *N* homogeneous isotropic inclusions (denoted *I*) with an elastic tensor $\boldsymbol{C}^{I}$. Both the TPU matrix and the DAPA inclusions display linear elastic properties. For a homogeneous isotropic material, the elastic tensor is expressed by eq. (4).

$$C_{ijkl}=2\mu\left[\left(\frac{v}{1\text{-}2v}\right)\delta_{ij}\delta_{kl}+\frac{1}{2}\left(\delta_{ik}\delta_{jl}+\delta_{il}\delta_{jk}\right)\right] \quad (4)$$

where μ and v represent the shear modulus and the Poisson ratio, respectively. In this study, the prediction of the elastic properties of the composite has been divided into two steps.

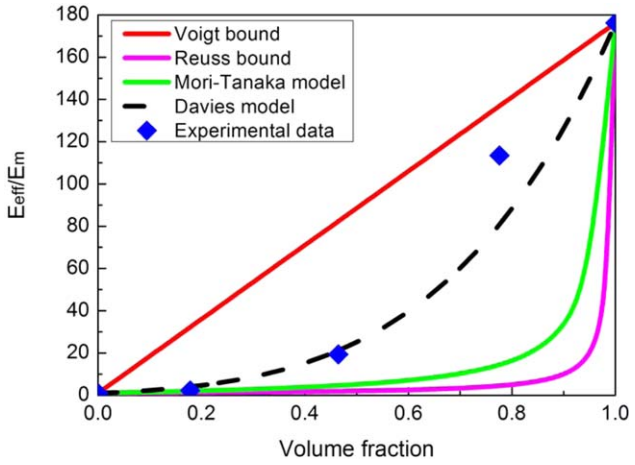

Figure 7. Evolution of the Young's modulus as a function of the DAPA volume fraction, comparison between experimental data and model predictions. [Color figure can be viewed in the online issue, which is available at wileyonlinelibrary.com.]

Table VI. Young Modulus and Poisson Ratio Obtained from the Mori–Tanaka and Davies Models

DAPA content (wt %)	Young's modulus (MPa)		Poisson ratio	
	Mori-Tanaka	Davies model	Mori-Tanaka	Davies model
0	1.5	1.5	0.43	0.43
20	3.1	7.5	0.39	0.43
50	7.6	39.6	0.35	0.43
80	24.1	137.5	0.31	0.43
100	264.2	264.2	0.32	0.32

First, the effective elastic properties of the TPU/DAPA blends have been determined. These effective properties have then been used as the matrix properties in HAR and $CaCO_3$-based composites. The effective elastic properties of the TPU/DAPA systems (blends and composites) were modelled using various approaches, such as Voigt,[35] Reuss,[36] Davies,[16] and Mori–Tanaka[15,37] models.

Voigt bound results in a deformation approach in which the strain is assumed to be constant in all the composite phases and equal to the imposed macroscopic deformation. The resulted equivalent stiffness tensor is given by the following expression: $C^{Voigt}=C^M+V_f(C^I\text{-}C^M)$, where V_f represents the inclusions volume fraction.

In the Reuss approach, the stress is assumed to be constant in all the composite phases and equal to the imposed macroscopic stress. The equivalent compliance tensor is then given by $S^{\text{Reuss}}=S^M+V_f(S^I\text{-}S^M)$, where S^M and S^I represent the matrix and the inclusion compliance tensors.

In the Mori–Tanaka model, the filler is supposed to be embedded in an infinite matrix that has the same properties than the matrix. The equivalent elastic tensor for the Mori–Tanaka model is given by the following equation: $C^{MT}=C^M+V_f(C^I-C^M)A^{MT}$, where $A^{MT}=A^{\text{Eshelby}}\left[(1-V_f)I+V_fA^{\text{Eshelby}}\right]^{-1}$ defining the Mori-Tanaka strain concentration tensor, $A^{Eshelby}=\text{I}+\text{S}(C^M)^{-1}(C^I-C^M)^{-1}$ is the Eshelby strain concentration tensor and **S** is the fourth dimension Eshelby strain tensor that depends on the matrix properties and the filler's geometrical shape.

The last model used in this study is the one well known to fit co-continuous structures without any specified details. This model, also known as the Davies model, is given by the empirical relation, $C^{\text{Davies}}=(C^M)^{1/5}\ (1-V_f)+(C^I)^{1/5}V_f$.

According to the SEM observations (Figure 2), the DAPA particles are well dispersed and are depicted as spherical inclusions

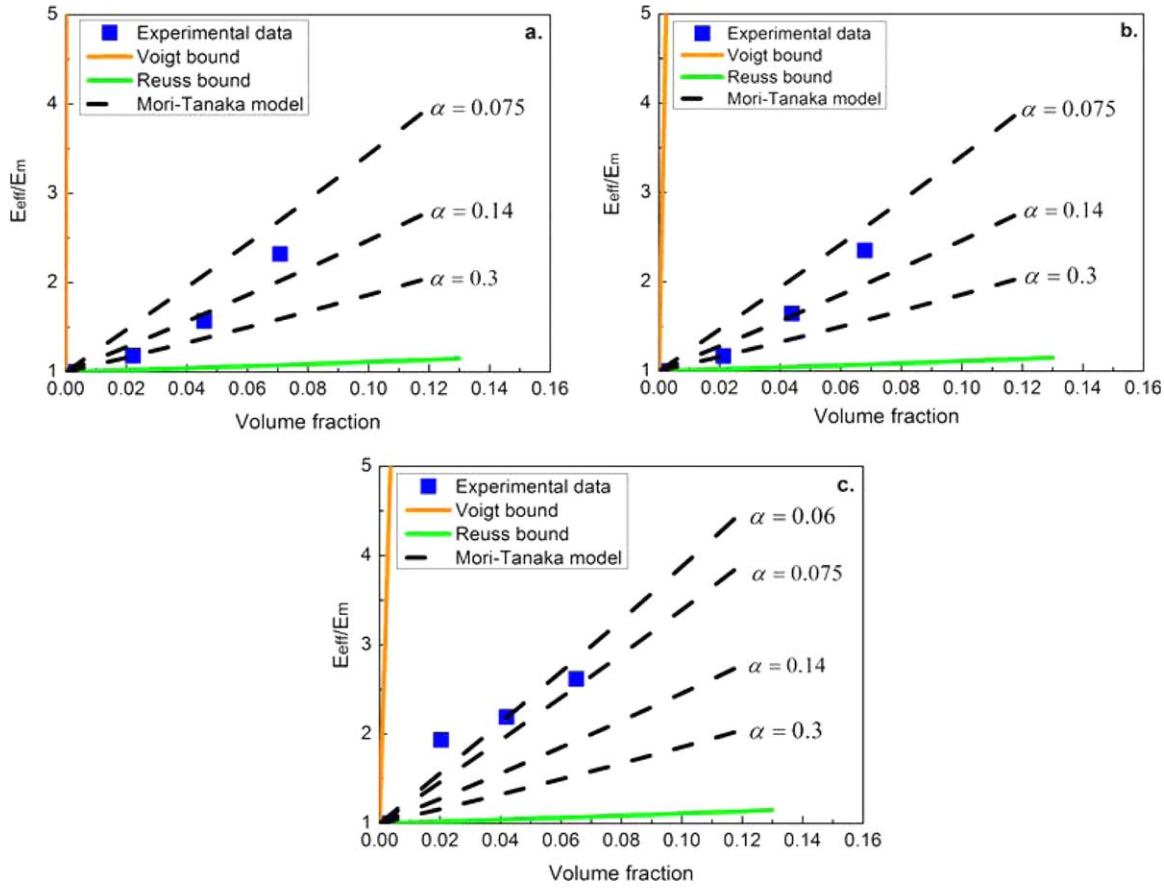

Figure 8. Evolution of the Young's modulus as a function of the HAR volume content, comparison between experimental data and predictions for (a) TPU/DAPA (80/20)_HAR, (b) TPU/DAPA (50/50)_HAR and (c) TPU/DAPA (20/80)_HAR. [Color figure can be viewed in the online issue, which is available at wileyonlinelibrary.com.]

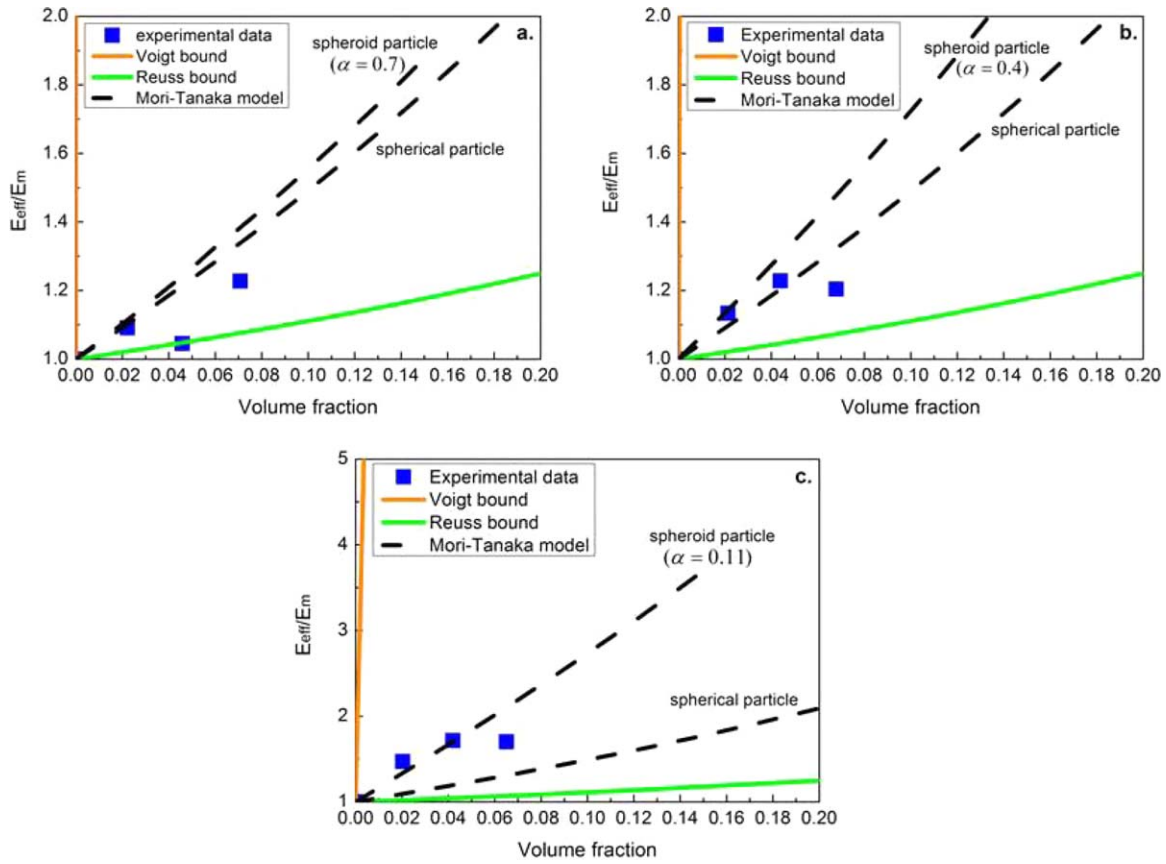

Figure 9. Evolution of the Young's modulus as a function of $CaCO_3$ volume fraction, comparison between experimental data and model predictions for (a) TPU/DAPA (80/20)_$CaCO_3$, (b) TPU/DAPA (50/50)_$CaCO_3$ and (c) TPU/DAPA (20/80)_ $CaCO_3$. [Color figure can be viewed in the online issue, which is available at wileyonlinelibrary.com.]

in the TPU matrix. In this particular case of spherical inclusions, the Eshelby tensor is expressed by eq. (5).

$$S_{ijkl} = \frac{5v-1}{15(1-v)}\delta_{ij}\delta_{kl} + \frac{4-5v}{15(1-v)}\left(\delta_{ik}\delta_{jl} + \delta_{il}\delta_{jk}\right) \quad (5)$$

Considering the Young's modulus $E_{TPU} = 1.5$ MPa and $E_{DAPA} = 264.2$ MPa, Poisson ratio $v_{TPU} = 0.43$ and $v_{DAPA} = 0.32$ for the TPU matrix and the DAPA inclusions respectively, the effective Young's modulus and Poisson ratio can be predicted.

The different numerical results have been compared to the experimental data (Figure 7) obtained by uniaxial tensile tests. As expected, the experimental data of the TPU/DAPA system stands between the Voigt and Reuss bounds. The Mori–Tanaka model allows a good prediction for low volume fractions (<0.2). The Davies model prediction is fairly in agreement with experimental data. All the effective properties (Young modulus and Poisson ratio) are reported in Table VI.

Both HAR and $CaCO_3$-based composites are considered as a two-phase material, composed by a matrix (TPU/DAPA) and inclusions (HAR or $CaCO_3$). We assume that all materials including the TPU/DAPA matrix and the HAR or $CaCO_3$ inclusions exhibit an isotropic elastic behavior. Because the Davies model brings the best predictions, both Young's modulus and Poisson ratio of TPU/DAPA can be determined by this model (Table VI). According to the SEM observations [Figure 1(b)], the HAR inclusions are in the TPU/DAPA matrix as spheroid oblate fillers. As previously mentioned and shown by SEM, the $CaCO_3$ particles present a spherical shape. The Eshelby tensor for spherical inclusions has been previously mentioned in relation to spheroid oblate shapes, the component of this tensor is given in the SI. The Young's modulus of HAR inclusion is $E_{HAR} = 70$ GPa and his Poisson ratio $v_{HAR} = 0.2$ while the $CaCO_3$ filler has a Young's modulus of $E_{CaCO3} = 72$ GPa and a Poisson ratio of $v_{CaCO3} = 0.2$.[38]

Figure 8 and Figure 9 show the results obtained by the Voigt, Reuss and Mori-Tanaka models (for different aspect ratios) and experimental data. As expected, the experimental data are located between the Voigt and Reuss bounds. The aspect ratio of the HAR fillers plays an important role on the elastic properties of the composite. As expected (Figure 8), the Young's modulus increases with the aspect ratio. For (80/20) and (50/50) systems, a good correlation between the predictions and the experimental data is obtained for $\alpha = 0.14$. With the $CaCO_3$ fillers (Figure 9), the Mori-Tanaka model predictions are in good agreement with the experimental data of the (80/20)_$CaCO_3$ and (50/50)_$CaCO_3$ composites. When the DAPA concentration is high, as in the case of (20/80)_$CaCO_3$, the Mori-Tanaka model for spherical inclusions underestimates the experimental

data. Good predictions in this particular case are obtained when the $CaCO_3$ fillers are assumed to be oblate spheroids with low aspect ratio ($\alpha = 0.11$). Even considering two phases, the Mori–Tanaka model gives good prediction results.

CONCLUSION

Bio-based composites prepared with thermoplastic blends and microfillers are obtained by a melting process. According to SEM images, mineral particles are well dispersed in each composite. After the addition of $CaCO_3$ or HAR, no noticeable changes on the TPU/DAPA morphologies of the blends are observed. From thermodynamic calculations combined with SEM images, we have been able to localize the mineral particles in the composites. For the 20/80 and 80/20 systems the microfillers are distributed in the major phase. For the 50/50 composites $CaCO_3$ particles are mainly located in the DAPA phase and HAR at the TPU/DAPA interface. Thermal analyses show that the crystallinity content of all the composites based on $CaCO_3$ and (80/20)_HAR systems has been decreased possibly due to a restriction of the mobility brought by the microfillers, which prevent crystal growth. It has been shown that the best fillers/matrix interactions are obtained for the multiphase systems based on DAPA as the main phase (20/80). Tensile tests show a conventional increase in the Young's modulus and yield stress with the addition of HAR and $CaCO_3$ particles. However, the increase in mechanical properties is much higher for composites with HAR microparticles, at same filler content, even if the moduli of HAR and $CaCO_3$ are comparable. This is due to a higher aspect ratio of HAR, which exhibits an interfacial surface almost 15 times greater than $CaCO_3$. Concerning the modeling of the results of the uniaxial tensile test, the two-phase Mori-Tanaka and Davies models give good predictions of the elastic properties. The Mori-Tanaka model also reveals that the aspect ratio of the HAR fillers played a predominant rule in the enhancement of the elastic properties. The use of a three-phase model (in which in the presence of an interphase is assumed) could be more accurate and enable the description of composites with poor adhesion between the polymer matrix and fillers. Such approaches are under investigation.

The association of bio-based polymers with fillers is a good solution to overcome primary issues with green polymers i.e., the material cost and/or the mechanical properties. These bio-based systems could find applications in different fields such as automotive or coating industry for long term usage.

ACKNOWLEDGMENTS

The authors thank Imerys Talc (France) and Omya (France) for providing talc and calcium carbonate samples. They are also grateful to Bpi-France and ANRT for their financial supports.

REFERENCES

1. Patel, M.; Bartle, I.; Bastioli, C.; Doutlik, K.; Ehrenberg, J.; Johansson, D.; Käb, H.; Klumpers, J.; Luther, R.; Wittmeyer, D. *Agro Food Ind. Hi-Tech* **2002**, *13*, 28.
2. Hablot, E.; Zheng, D.; Bouquey, M.; Avérous, L. *Macromol. Mater. Eng.* **2008**, *293*, 922.
3. Hablot, E.; Donnio, B.; Bouquey, M.; Avérous, L. *Polymer* **2010**, *51*, 5895.
4. Bueno-Ferrer, C.; Hablot, E.; Garrigós, M. C.; Bocchini, S.; Avérous, L.; Jiménez, A. *Polym. Degrad. Stab.* **2012**, *97*, 1964.
5. Bueno-Ferrer, C.; Hablot, E.; Perrin-Sarazin, F.; Garrigós, M. C.; Jiménez, A.; Avérous, L. *Macromol. Mater. Eng.* **2012**, *297*, 777.
6. Fan, X. D.; Deng, Y.; Waterhouse, J.; Pfromm, P. *J. Appl. Polym. Sci.* **1998**, *68*, 305.
7. Reulier, M.; Avérous, L. *Eur. Polym. J.* **2015**, *67*, 418.
8. Sepulcre-Guilabert, J.; Ferrándiz-Gómez, T. P.; Martín-Martínez, J. M. *J. Adhes. Sci. Technol.* **2001**, *15*, 187.
9. Demjén, Z.; Pukánszky, B.; Földes, E.; Nagy, J. *J. Colloid Interface Sci.* **1997**, *190*, 427.
10. Demjén, Z.; Pukánszky, B.; Nagy, J. *Compos. A* **1998**, *29*, 323.
11. Leong, Y. W.; Abu Bakar, M. B.; Ishak, Z. A. M.; Ariffin, A.; Pukanszky, B. *J. Appl. Polym. Sci.* **2004**, *91*, 3315.
12. Moussa, M. A.; Ghoneim, A. M.; Hakim, A. A. A.; Turky, G. M. *Adv. Polym. Technol.* **2009**, *28*, 257.
13. Beuguel, Q.; Ville, J.; Crepin-Leblond, J.; Mederic, P.; Aubry, T. *Polymer* **2015**, *62*, 109.
14. Leterme, P.; Gayot, A.; Finet, G.; Bizi, M.; Flament, M. P. *Int. J. Pharm.* **2005**, *289*, 109.
15. Mori, T.; Tanaka, K. *Acta Metall.* **1973**, *21*, 571.
16. Davies, W. E. A. *J. Phys. D Appl. Phys.* **1971**, *4*, 1325.
17. Van Krevelen, D. W. Properties of Polymers: Their Correlation with Chemical Structure; Their Numerical Estimation and Prediction from Additive Group Contributions, Third Completely Revised Edition; Elsevier: Amsterdam, **1997**.
18. Wu, S. *J. Polym. Sci. C Polym. Symp.* **1971**, *34*, 19.
19. Dalal, E. N. *Langmuir* **1987**, *3*, 1009.
20. Bismarck, A.; Kumru, M. E.; Springer, J. *J. Colloid Interface Sci.* **1999**, *217*, 377.
21. Taguet, A.; Cassagnau, P.; Lopez-Cuesta, J. M. *Prog. Polym. Sci.* **2014**, *39*, 1526.
22. Fenouillot, F.; Cassagnau, P.; Majesté, J. C. *Polymer* **2009**, *50*, 1333.
23. Ivan Javni, Z. S. P.; Guo, A.; Fuller, R. *J. Appl. Polym. Sci.* **2000**, *77*, 1723.
24. Levchik, S. V.; Weil, E. D. *Polym. Int.* **2004**, *53*, 1585.
25. Saunders, J. H. *Rubber Chem. Technol.* **1959**, *32*, 337.
26. Krol, P. *Prog. Mater. Sci.* **2007**, *52*, 915.
27. Alonso, M.; Gonzalez, A.; De Saja, J. A.; Escalona, A. M. *Thermochim. Acta* **1991**, *184*, 125.
28. Georgieva, V.; Vlaev, L.; Gyurova, K. *J. Chem.* **2013**, *2013*, 12.
29. Jašo, V.; Cvetinov, M.; Rakić, S.; Petrović, Z. S. *J. Appl. Polym. Sci.* **2014**, *131*.
30. Zhang, S. L.; Wang, G. B.; Jiang, Z. H.; Wu, W. C.; Ma, R. T.; Wu, Z. W. *J. Appl. Polym. Sci.* **2004**, *94*, 839.
31. Wang, X.; Luo, X.; Wang, X. *Polym. Test.* **2005**, *24*, 18.

32. Yousfi, M.; Livi, S.; Dumas, A.; Crépin-Leblond, J.; Greenhill-Hooper, M.; Duchet-Rumeau, J. *J. Appl. Polym. Sci.* **2014**, *131*.

33. Kodal, M.; Erturk, S.; Sanli, S.; Ozkoc, G. *Polym. Compos.* **2015**, *36*, 739.

34. Bajsic, E. G.; Rek, V.; Pavic, B. O. *J. Elastomer Plast.* **2013**, *45*, 501.

35. Voigt, W. Lehrbuch der Kristallphysik (mit Ausschluss der Kristalloptik); Vieweg+Teubner Verlag: Berlin, **2014**.

36. Reuss, A. *J. Appl. Math. Mech.* **1929**, *9*, 49.

37. Mortazavi, B.; Baniassadi, M.; Bardon, J.; Ahzi, S. *Compos. B* **2013**, *45*, 1117.

38. Jančař, J. *J. Mater. Sci.* **1989**, *24*, 3947.